Journal of Materials Chemistry A

PAPER

View Article Online
View Journal | View Issue

Cite this: J. Mater. Chem. A, 2016, 4, 944

Multihierarchical electrodes based on titanate nanotubes and zinc oxide nanorods for photoelectrochemical water splitting†

J. S. Souza,[ab] W. M. Carvalho, Jr.,[a] F. L. Souza,[a] C. Ponce-de-Leon,[b] D. V. Bavykin*[b] and W. A. Alves*[a]

Received 24th August 2015
Accepted 28th November 2015

DOI: 10.1039/c5ta06646h

www.rsc.org/MaterialsA

Studies involving water splitting to form hydrogen and oxygen have attracted attention because H_2 is considered the fuel of the future. Photoelectrocatalysts have been widely used for this application, and several metal oxides can be applied as catalysts. Among them, we highlight zinc oxide nanorods (ZnONRs) and titanate nanotubes (TiNTs); however, their individual nanostructures exhibit disadvantages. For example, ZnONRs show rapid recombination of the photogenerated charges, and TiNTs give rise to randomly oriented films; these disadvantages limit their application as photoanodes. In this study, for the first time, we present a new class of multihierarchical electrodes based on TiNT-decorated ZnONR films that exhibited superior results to the individual species. The TiNTs are homogenously dispersed over the surface of the rods without forming agglomerates, giving rise to a heterojunction that exhibits lower recombination rates. It was found that the results are better when the contents of TiNTs in the electrode are higher; thus, glycine was successfully used as a bridge to link both of the structures, increasing the amount of TiNTs decorating the rods. As a result, the photocurrent generated with these multihierarchical electrodes is higher than that obtained with pure ZnONR electrodes (0.9 mA cm^{-2} and 0.45 mA cm^{-2} at 1.23 V_{RHE}, respectively), and the electrode potentials for O_2 evolution are lower than those observed for pure TiNT electrodes (0 V and 0.8 V *vs.* E_{RHE}, respectively). The IPCE values are also higher for the multihierarchical electrodes.

Introduction

Hydrogen, which is considered the fuel of the future, has attracted extensive attention because it is environmentally friendly and is an energy carrier with a very high energy density.[1] Photoelectrocatalytic water splitting using sunlight is an interesting approach for producing H_2 and O_2; however, the chosen photocatalyst must fulfill certain requirements, such as optimal band gap levels (aligned with the energy required to perform the reactions of H_2/H_2O and O_2/H_2O), high stability and low recombination rates.[2] Since TiO_2 photoelectrodes were first used for the water splitting reaction,[3] many other catalysts based on metal oxides have been investigated, especially those involving nanomaterials.[4–7] Among them, we highlight titanate nanotubes (TiNTs – see Table 1), which exhibit an open and mesoporous morphology, high surface area, wide band gap energy and good electrical conductivity.[8] Zinc oxide nanorods (ZnONRs) have also been extensively used as photocatalysts for H_2 and O_2 production from water because of their wide band gap energy, high electron mobility and low charge recombination due to the longer electron lifetimes.[9] These properties make TiNTs and ZnONRs more promising photocatalysts compared with other widely studied materials, such as platinum-group catalysts, which are expensive, as well as catalysts for the conversion of H_2 and O_2 back to water,[2] and Fe_2O_3, which exhibits low electron conductivity and high electron–hole recombination rates[10–13]. Table 1 summarizes recent advances involving the application of TiNTs and ZnONRs for the development of photocatalysts and photoanodes for water splitting experiments.

However, TiNTs and ZnONRs exhibit disadvantages for water splitting applications, including low photonic efficiency and reduced visible-light absorption, which prevent significant utilization of the solar spectrum. The design of systems involving the heterojunction of these two nanomaterials is an interesting approach since it has been already reported in the literature that the synergic effect caused by the combination of metal oxides can improve the photocatalytic activity by lowering the recombination rates.[14,15]

For use as photoanodes in photoelectrocatalysis, these materials must be immobilized on a conductive surface, which

[a]Centro de Ciencias Naturais e Humanas, Universidade Federal do ABC, 09210-580, Santo André, São Paulo, Brazil. E-mail: wendel.alves@ufabc.edu.br

[b]Energy Technology Research Group, Faculty of Engineering and the Environment, University of Southampton, UK. E-mail: D.Bavykin@soton.ac.uk

† Electronic supplementary information (ESI) available. See DOI: 10.1039/c5ta06646h

Table 1 Bibliographic review for TiNTs and ZnONRs applied to water splitting

Photoelectrocatalysis

Catalyst	H_2 evolution (μmol g^{-1})	Irradiation source	Ref
CdS/TiNT	175 after 3 h	λ > 420 nm 150 W	24
CdS/TiNT/WO_3	350 after 3 h	λ > 420 nm 150 W	24
Graphene /TiNT	60 after 5 h	300 W Xe-lamp	25
CdS/TiNT	100 after 10 h	λ > 420 nm 300 W xenon	26
CdS/TiNT	5000 after 18 h	150 W Xe arc lamp	27
Cr_2O_2/TiNT	4575 (μL g^{-1}) after 6 h	λ > 400 nm 350 W xenon	28
CdS/TiNT	1800 (μL g^{-1}) after 6 h	λ > 400 nm 350 W xenon	29

Photoelectrocatalysis

Catalyst	Substrate	Current (mA cm^{-2}) *vs.* E_{RHE} 1.23	Start potential (V)	Irradiation source	Ref
Fe_2O_3/TiNT	FTO	4.00	0.8	100 mW cm^{-2} UV/vis irradiation (Hg–Xe 200 W)	12
Fe_2O_3/TiNT	FTO	4.00	0.8	100 mW cm^{-2} UV/vis irradiation (Hg–Xe 200 W)	30
HTiNT	FTO	0.04	1.5	UV 150 mW cm^{-2}	31
Cu_2O/ZnONR	FTO	1.35	−0.4	AM 1.5G	32
ZnONR	ITO	1.6	0.0	AM 1.5G	33
MWCNT/ZnONR	FTO	1.5	0.0	AM 1.5G	34
Au/ZnONR	Zn foil	2.2	0.0	AM 1.5G	35
Ni/ZnONR	FTO	0.9	−0.4	150 W Xe arc lamp	36
Au/ZnONR	FTO	1.3	−0.2	AM 1.5G	37
Cu_xO/ZnONR	FTO	0.6	0.0	AM 1.5G	38
Au/ZnONR	PET	2.2	−0.25	UV 100 mW cm^{-1}	39

is a challenge for TiNTs because all of the strategies used for this goal resulted in films in which the nanotubes are randomly oriented and packed in a dense film layer, which can especially affect the electron transport[8,16–18]. For this reason TiNTs have been used mostly as photocatalysts for water splitting in the powder form, as is shown in the upper part of Table 1. However, vertically aligned ZnO nanorod films can be easily obtained through several methods, such as hydrothermal synthesis, which is an inexpensive technique that requires low temperature, and the films can grow on several different surfaces without requiring metal catalysts.[9,19–23]

Thus, we propose the design of an electrode based on TiNT and ZnONR materials on the nanoscale, by developing a multiscale hierarchical electrode for efficient oxygen evolution *via* photoelectrochemical water splitting, which follows the trend of recent developments and applications of composite nanomaterials. This strategy can synergistically contribute to the advantages of their individual components, thereby reducing their shortcomings.[40–42]

ZnONRs develop a positive zeta potential,[43] and titanate nanotubes have a relatively large negative zeta potential in water,[44] favoring the preparation of a multiscale hierarchical electrode composed of these two materials by simply mixing them and using the opposite zeta potentials to adhere them together. However, the interaction between TiNTs and ZnONRs was not strong enough to form decorated films with a high amount of TiNTs. To improve the interaction, we decided to use a bridge to link these two nanomaterials. Glycine was chosen to play this role because it is known that the surface of ZnONRs has a good affinity to carboxylic groups,[45–47] whereas the TiNT surface can form strong bonds with amino groups.[48] Few studies involving ZnO and glycine[49–52] and TiNT modification with glycine[53] were reported in the literature.

This study describes a novel class of multihierarchical electrodes based on TiNTs and ZnONRs obtained *via* a simple two-step method. This strategy allowed us to (i) overcome the TiNT agglomeration issue, (ii) increase the surface area of the interface between semiconductors and liquid solvent and (iii) maintain the open pore structure of the solid electrode. Additionally, we report an enhancement of the charge separation observed by an increased photoelectrocatalytic response using the multihierarchical electrodes, as photoanodes for water splitting under sunlight conditions.

Experimental

Multihierarchical electrode preparation procedure

Reactants. Zinc nitrate hexahydrate $Zn(NO_3)_2 \cdot 6H_2O$, hexamethylenetetramine (HMT) and glycine (gly) were obtained from Sigma-Aldrich and were used without further purification. Titanate nanotubes were prepared using an alkaline hydrothermal process according to the literature with minor modifications.[54,55]

ZnONR and ZnONR + gly films. FTO glass was used as the substrate to grow the ZnONR and ZnONR + gly films. Substrates with dimensions of 2.5 × 4.0 cm were cleaned three times by

sonication in ethanol, deionized water and acetone for ten minutes. To grow the films, a two-step method based on the literature with minor modifications was used.[56] First, a seed layer was prepared by dripping aqueous solutions of $Zn(NO_3)_2$ (1.5 mL, 0.5 mol L^{-1}) and HMT (1.5 mL, 0.5 mol L^{-1}) on the substrates. After 5 min of deposition, the substrates were spin coated for 6 s at 500 rpm and then for 30 s at 3000 rpm. Finally, they were dried and annealed at 210 °C for 15 min. ZnONR films were grown in a second step using a hydrothermal method by soaking the modified substrates in a mixture of $Zn(NO_3)_2$ (0.1 mol L^{-1}) and HMT (0.1 mol L^{-1}), maintaining their volume ratio at 1 : 1. The hydrothermal growth was performed at 100 °C for 4 h in a sealed beaker. To grow ZnONR + gly films, glycine was added to the growth mixture, while maintaining the molar ratio of Zn : gly at 5 : 1.

Preparation of TiNT and TiNT + gly suspension. For the preparation of a stable suspension of titanate nanotubes, 100 mg of TiNT was suspended in 100 mL of deionized water by sonication for 3 h using an UltraSonic Cleaner – SW2000FI (Sanders); the sonication also helps to reduce the length of TiNTs.[57] After allowing the suspension to stand for 24 h, the precipitate was separated from the stable colloid by decanting. The concentration of titanium in the TiNT suspension was estimated as 5 mmol L^{-1}, according to procedures previously described in the literature.[17] To prepare titanate nanotubes modified with glycine (TiNT + gly), the TiNT suspension was stirred with gly (molar ratio of 1 : 1 – Ti : gly) for 30 min at room temperature.

Decoration of ZnONR films with TiNTs. The TiNT suspension was diluted to 2.0 mmol L^{-1} in a mixture of deionized water and ethanol (1 : 1). The ZnONR film was soaked in the obtained suspension under stirring for 30 min at room temperature. The resultant film was dried in air to form the ZnONR film decorated with TiNT (TiNT → ZnONR). The same procedure was used to decorate ZnONR + gly films with the TiNT suspension to obtain TiNT → ZnONR + gly films. Finally, the TiNT + gly suspension was used to decorate ZnONR films, forming TiNT + gly → ZnONR. In this procedure, the TiNT + gly suspension was diluted to 2.0 mmol L^{-1}, and then the procedure previously described was followed to obtain the TiNT → ZnONR film.

Table 2 summarizes the electrode labels as a function of their preparation conditions; these names are used throughout the text.

Adsorption of methylene blue (MB) over TiNT was used to quantify the amount of nanotubes present on the multi-hierarchical electrodes. Decorated films were dipped in a 0.01 mol L^{-1} MB solution for 8 h, and then the absorbance of MB was measured using a UV-vis spectrometer (double beam UV-vis Spectrophotometer – Sinco).

Table 2 Electrode labels and preparation conditions

Preparation conditions		Obtained electrode labels
Nanotube suspension	Nanorod film	
TiNT (2.0 mmol L^{-1})	ZnONR	TiNT → ZnONR
TiNT + gly (2.0 mmol L^{-1})	ZnONR	TiNT + gly → ZnONR
TiNT (2.0 mmol L^{-1})	ZnONR + gly	TiNT → ZnONR + gly

Structural and physical characterization

Scanning electron microscopy (SEM) images were obtained using an SEM-FEG HR Inspect F50 (FEI) scanning electron microscope, located at the Laboratory of Electron Microscopy of the Nanotechnology National Laboratory, Campinas, Brazil. The electronic transmission microscopy (TEM) and Energy Dispersive X-Ray (EDX) analysis were conducted using a TECNAI F20 FEI microscope, operating at 200 kV. The TEM images and EDX images of TiNT–ZnONRs were obtained by removing the formed film from the substrate with a scalpel blade. The removed powder was dispersed in isopropyl alcohol and dripped on a carbon coated copper grid. The crystalline phase of ZnONR and ZnONR + gly films was determined by powder X-ray diffraction (XRD) using a D8 (FOCUS) X-ray spectrometer equipped with a Cu Kα radiation source operating at 40 kV and 40 mA. The XRD profiles were collected between 5° and 70°. Zeta potential analyses (ζ-potential) were performed using a Zetasizer Nano ZS (Malvern) with high concentrated suspensions of the samples in water. The films' surface hydrophobicity was determined by measuring the water contact angle (WCA) using a WCA analyzer (DigiDrop MCAT, GBX).

Electrochemical and photoelectrochemical measurements

Electrochemical measurements were performed in a three-electrode cell with a quartz window coupled with a potentiostat/galvanostat (μAutolab III). For these analyses, the pure and modified ZnO films were used as the working electrodes, Ag/AgCl in saturated KCl as the reference electrode and platinum foil as the counter electrode. The measured potentials *vs.* Ag/AgCl were converted to the reversible hydrogen electrode (RHE) scale according to eqn (1):

$$E_{RHE} = E_{Ag/AgCl} + 0.059\ pH + E^{\circ}_{Ag/AgCl}, \quad (1)$$

where E_{RHE} is the converted potential *vs.* RHE, $E^{\circ}_{Ag/AgCl} = 0.1982$ V at 25 °C, and $E_{Ag/AgCl}$ is the potential experimentally measured against the Ag/AgCl reference electrode. An aqueous solution of 0.01 mol L^{-1} Na_2SO_4 (pH 7.9, Sigma-Aldrich, 99.9%) was used as the electrolyte. Linear sweep voltammetry (current density *vs.* applied potential) was performed in the dark and under sunlight-simulated conditions at a scan rate of 50 mV s^{-1}.

Chronoamperometry (current *vs.* time) was performed at 1.23 V_{RHE} under sunlight-simulated conditions. The sunlight-simulated conditions were obtained using a 450 W xenon lamp (Osram, ozone free) and an AM 1.5 filter. The light intensity was set to 100 mW cm^{-2}.

The incident photo-to-current conversion efficiency (IPCE) was measured as a function of the excitation wavelength (λ) using a 300 W xenon-ozone free lamp coupled to a cornerstone 260 monochromator (Oriel Quantum Efficiency Measurement Kit). The IPCE was calculated using the following equation:

$$\mathrm{IPCE} = (I(\lambda)1240/E(\lambda)\lambda)100, \quad (2)$$

where $I(\lambda)$ is the photocurrent density (μA cm^{-2}), and $E(\lambda)$ is the irradiance (μW cm^{-2}).

Results and discussion

Multihierarchical electrode characterization

SEM images of ZnONR (Fig. 1a) and ZnONR + gly films (Fig. S1†) show that the rods have a hexagonal shape and their surface is very smooth which is consistent with that described in the literature.[9,19–23] The average diameters of the rods are 490 nm and 400 nm for the ZnONR and ZnONR + gly films, respectively. The ZnONR film also exhibits better vertical alignment and higher density than the ZnONR + gly film.

TiNTs are much smaller than ZnONRs; therefore, it is possible to decorate each rod with several nanotubes, which can be seen in the SEM images of TiNT → ZnONR, TiNT + gly → ZnONR and TiNT → ZnONR + gly films (Fig. 1b–d). The images also revealed that the TiNTs are homogeneously dispersed along the rods without forming agglomerates, which is very common when other methods to obtain TiNT films are used.

The amount of TiNTs decorating these films was measured by an indirect method involving MB. In aqueous solution the dye experiences electrolytic dissociation resulting in cationic species, therefore they strongly adsorb on the surface of TiNTs which develop a negative zeta potential.[58] Absorbance spectra of all samples were recorded (Fig. S2†) and the absorption of the dye was measured at its maximum absorption of 654 nm. The difference in absorbance between MB-coated multihierarchical films and non-decorated ZnONR and ZnONR + gly films (ΔA) was determined, revealing that the amount of nanotubes decorating the rods increases in the following order: TiNT → ZnONR ($\Delta A = 0.0038$) < TiNT → ZnONR + gly ($\Delta A = 0.013$) < TiNT + gly → ZnONR (ΔA 0.017).

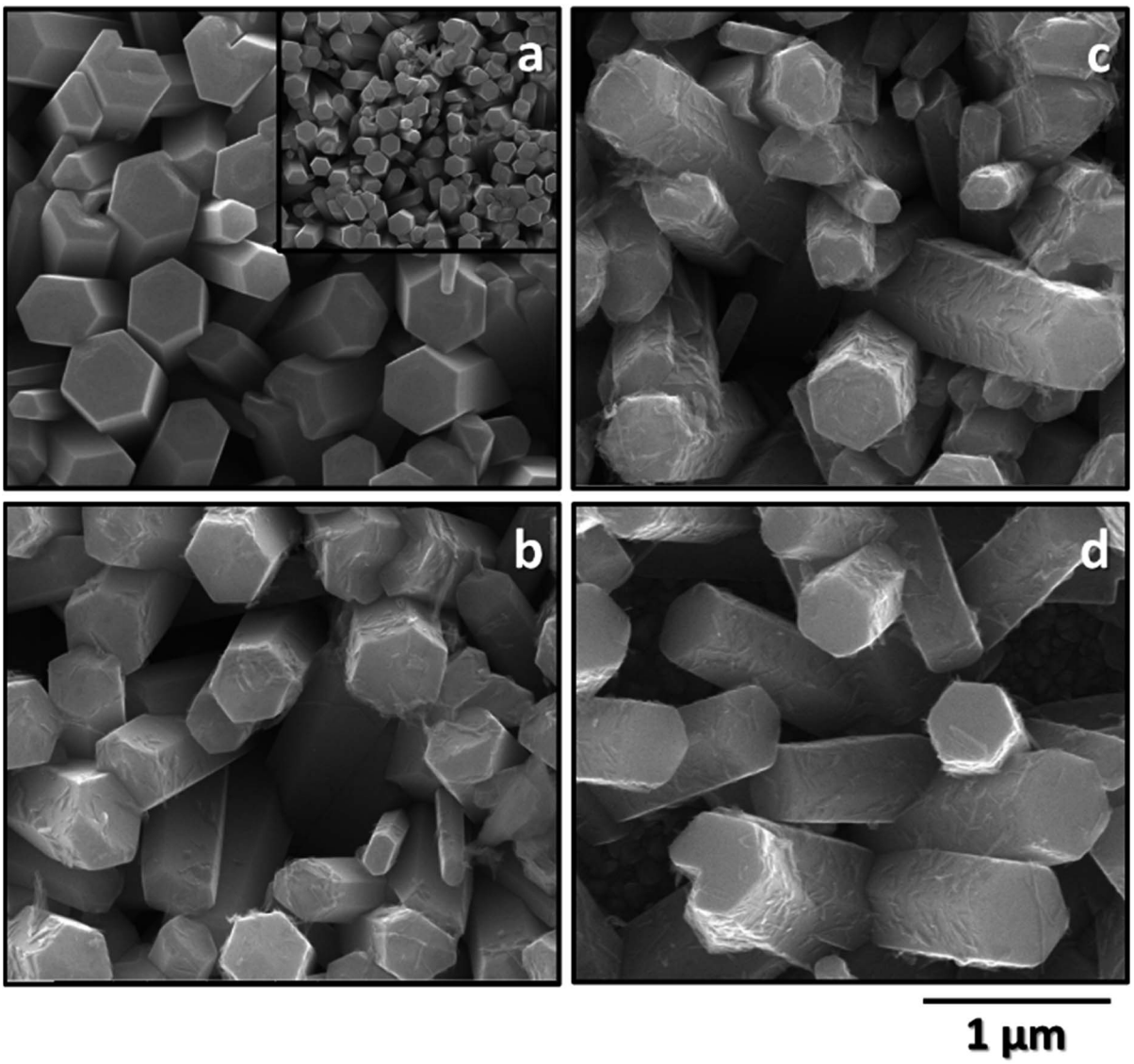

Fig. 1 SEM images of (a) ZnONR, (b) TiNT → ZnONR, (c) TiNT + gly → ZnONR, and (d) TiNT → ZnONR + gly films.

This result can be associated with the presence of glycine, which appears to change the zeta potential of the investigated nanomaterials, with values of +23.32 mV and +6.65 mV for ZnONR + gly and ZnONRs films, respectively, and −34.90 mV and −36.40 mV for TiNT and TiNT + gly, respectively. These results indicate that gly promoted changes over the surface composition, modifying its point of zero charge. This change is directly correlated with the zeta potential value;[59] thus, the modification of zeta potentials may increase the electrostatic interaction between rods and tubes. It is already known that the NH_3^+ and COO^- groups can chemically bond to ZnO and TiNT;[51–53] thus, gly can also act as a bridge linking the two structures through a strong chemical bond. These results show that glycine successfully played its role in increasing the interaction between the tubes and rods, resulting in films with a higher amount of TiNTs. The modification of TiNTs and ZnONRs with glycine was also proved by FT-IR spectroscopy, and the results are shown in the ESI in Fig. S3.†

The XRD patterns of ZnONR and ZnONR + gly films (Fig. 2) were compared with those available in the Inorganic Crystal Structure Database (ICSD) showing the wurtzite ZnO pattern (ICSD 26170 and 180050). The enhanced (002) peak results from the preferred c-axis orientation of the ZnO nanorods.[60,61]

The XRD patterns of the ZnONR and ZnONR + gly films are highly similar, showing only a small change in the relative intensity of peaks, which can be ascribed to the small difference in the length of the rods in each film. Besides, due to the thin thickness and relatively small mass fraction of TiNTs on the ZnONR surface, it was not possible to obtain an XRD signal with sufficient signal to noise ratio from the composite film edge. We have attached the typical XRD patterns of TiNT powder to the supplementary file for reference, and they are similar to those observed in the literature (see Fig. S4†).[62] In order to confirm the presence of TiNTs modifying the ZnONR surface TEM images of the TiNT + gly → ZnONR film (Fig. S5a†) were obtained, where it is possible to see the presence of thin TiNTs deposited over the ZnONR surface, indicated by the red arrows in the images. In addition, energy dispersive X-ray analysis (EDX, Fig. S6†) was carried out in the selected area (red dashed circle) shown in the TEM image (Fig. S5b and c†) to confirm that the TiNTs were successfully attached at the ZnONR surface.

The wettability of ZnONR and ZnONR + gly films with the electrolyte used in the electrochemical experiments (0.01 mol L^{-1} Na_2SO_4 in water) was measured and is displayed in Fig. 3. Contact angles of 78° and 98° were observed for ZnONR and ZnONR + gly, which are ascribed to hydrophilic and hydrophobic surfaces, respectively. This behavior can be related to film morphology (or roughness), which suggests an amount of air could be trapped within the interstices. This trapped air pressure balances the gravity, and the surface tension of the water is responsible for maintaining the spherical shape of the droplet.[57] The film with a higher volume of air (ZnONR + gly, see SEM images) effectively prevents the penetration of water droplets into the grooves, thereby increasing the hydrophobicity.

Electrochemical and photoelectrochemical studies

The obtained multihierarchical electrodes were applied as photoanodes in water splitting experiments. Fig. 4a exhibits the photocurrent density *versus* voltage (measured against a reversible hydrogen electrode as a reference) curves of all the electrodes in the presence and absence of sunlight-simulated irradiation (AM 1.5G).

The mechanism for water splitting in half of the photoelectrochemical cell, catalyzed either by TiNTs and ZnONRs, involves the oxidation of H_2O to form O_2 using the photogenerated holes.[63] In the dark, the e^- and h^+ are combined at the valence band of the semiconductors; thus, no catalytic effect is obtained, as can be observed for all electrodes, represented by the dashed lines in Fig. 4a. The O_2 evolution, in this case, is only observed when high potentials are applied (*via* electrolysis). When the complete device (composed of the multihierarchical electrodes and noble metal as the anode and cathode, respectively) is irradiated by light, the electrons from the valence band are promoted to the conduction band. Because E_{CB} is more negative than E_{H_2/H_2O} and E_{VB} values are more positive than E_{O_2/H_2O}[64,65] H_2 and O_2 are produced at a lower potential (approximately 0 V), and high currents are generated (solid lines in Fig. 4a). The capability of these systems is only demonstrated when irradiated with light, which is also proved in the chronoamperometry experiments in which the light is turned on and off at defined intervals. These results are shown in the ESI (Fig. S7†). Additionally, it has been found that glycine may improve the contact between the tubes and rods, consequently increasing the charge separation.[66] Aiming to prove that the

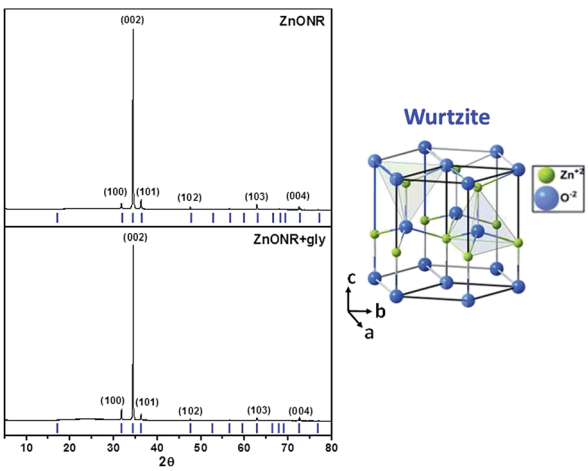

Fig. 2 XRD patterns of ZnONR and ZnONR + gly films and the crystalline structure of wurtzite.

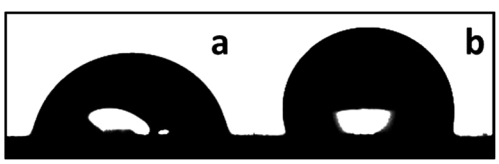

Fig. 3 Contact angle images of Na_2SO_4 0.01 mol L^{-1} aqueous solution droplet on the surface of (a) ZnONR and (b) ZnONR + gly films.

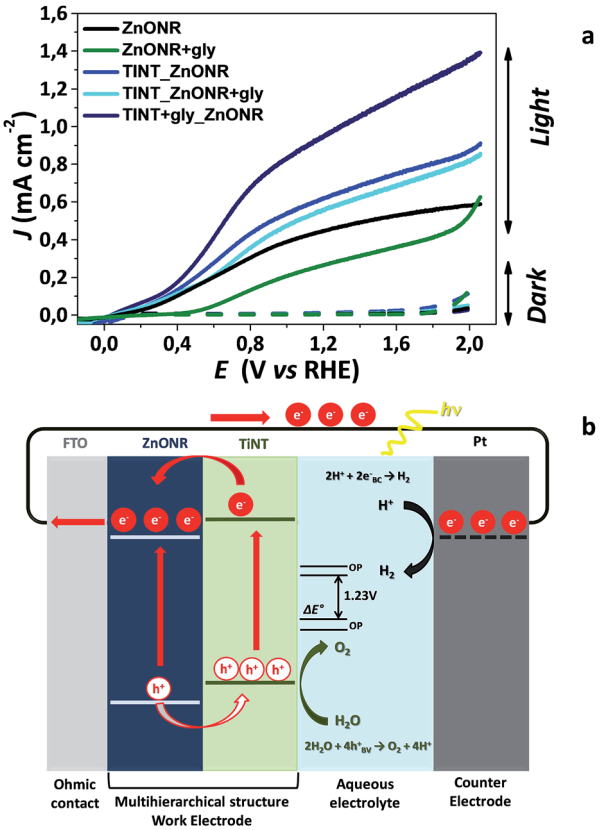

Fig. 4 (a) Photocurrent (*J*) *vs.* voltage (V_{RHE}) curves without and with sunlight irradiation, measured using a scan rate of 50 mV s^{-1}. Electrolyte: 0.01 mol L^{-1} Na_2SO_4; (b) schematic representation of photoelectrocatalytic water splitting using the TiNT/ZnONR-based multihierarchical electrodes.

increment of the current is not due to a RedOx process of glycine, gly solution was added to the electrolyte during a chronoamperometry experiment (see ESI†).

The current densities obtained for pure zinc oxide nanorods (ZnONRs and ZnONR + gly films) are lower than those observed for TiNT-decorated systems, which is a consequence of the faster charge recombination that occurs with pure ZnONRs. The formation of the heterojunction between nanotubes and nanorods increases the photostability of the electrodes due to the synergic contribution from the TiNTs to the ZnONRs. Fig. 4b shows a schematic representation of this synergism.

When multihierarchical electrodes are irradiated, electrons are photogenerated (either in TiNTs and ZnONRs) and are immediately transferred from the CB from TiNTs to the CB from ZnONRs due to the favorable potential difference between them. These electrons flow to the FTO films and then to the Pt counter-electrode, through the electrical contact, to be used in H^+/H_2 reduction. The holes remaining in the valence band of the two nanostructures are promptly transferred from the ZnONR to TiNT VB, which is also due to the favorable potentials,[14,63] and are used in the H_2O/O_2 reaction. Therefore, the formation of this heterojunction improved the charge separation, hindering the recombination of the photogenerated species and increasing the observed photocurrents. Thus, the photocurrent density is higher for the electrode with a higher content of TiNTs, which is the TiNT + gly → ZnONR electrode, as can be observed in the SEM images (Fig. 1c). The electrodes based on ZnONR + gly exhibit a lower response compared with electrodes based on ZnONR films. This can be attributed to their low wettability, which may affect the diffusion process (Fig. 3). The photocurrent values for all electrodes are summarized in Table 3.

In addition, the photocurrent density stability at an applied potential of 1.23 V_{RHE} under sunlight-simulated conditions was determined by chronoamperometry. Fig. 5a corresponds to the curves of photocurrent density *versus* time (60 min) for all electrodes under illumination. The films showed very good stability, which is an important requirement for their application in photoelectrochemical devices. However, TiNT → ZnONR + gly and ZnONR + gly, represented by cyan and green solid lines, respectively, in Fig. 5a, displayed an increasing behavior of photocurrent density dependence of time. This result can also be explained by their low wettability, indicating that these systems require more time in contact with the electrolyte to start the chemical reaction at the interface to generate photocurrent.

IPCE was measured at an applied potential of 1.23 V_{RHE} as a function of the wavelength (nm) for all electrodes. IPCE values for ZnONR (black line), ZnONR + gly (green line), TiNT + ZnONR (blue line), TiNT → ZnONR + gly (cyan line) and TiNT + gly → ZnONR (navy line) films were found to be approximately 20.0, 16.0, 76.0, 84.0 and 88.0% at 220 nm, and lower values of 18.0, 17.0, 20.0, 27.0 and 45.0% were observed at 360 nm, respectively (Fig. 5b). Consequently, the decorated film exhibited enhanced IPCE values at higher wavelengths, which can be related to the electron absorption changes caused by the heterojunction. This is also observed in the reflectance UV-vis spectra, presented in the ESI (Fig. S9†). In general, the decorated electrodes exhibit increased efficiency, which is also ascribed to the synergic effect between TiNTs and ZnONRs, which promotes higher photogenerated charge stability. Their photoelectrochemical performance was analyzed using two complementary techniques: (i) determination of IPCE and (ii) use of a sunlight simulator (Xe-lamp with an AM 15G filter). The sunlight simulator aids the evaluation of the electrode performance under real conditions. Using the IPCE measurements, we determine the wavelength that elicits the highest response (measured from 220 to 700 nm with a step of 10 nm). Then, it is mandatory to integrate the IPCE data with that obtained from a standard solar spectrum;

Table 3 Summarized values of photocurrent density for oxygen evolution obtained for all electrodes under sunlight irradiation

	J (mA cm^{-2})	
Electrodes	1.23 V_{RHE}	1.70 V_{RHE}
ZnONR	0.45	0.54
ZnONR + gly	0.27	0.38
TiNT → ZnONR	0.62	0.77
TiNT → ZnONR + gly	0.57	0.71
TiNT + gly → ZnONR	0.90	1.20

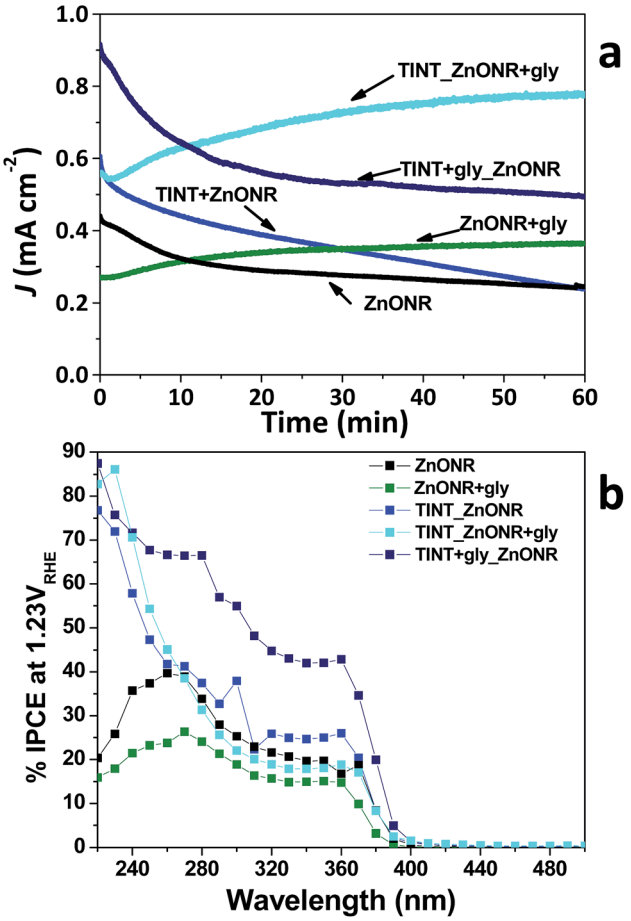

Fig. 5 (a) Chronoamperometry plots (*J vs.* time) performed at 1.23 V_{RHE}. (b) IPCE performed at 1.23 V_{RHE} for all electrodes. Electrolyte: 0.01 mol L^{-1} Na_2SO_4.

the overall photocurrent must be similar in both of the measurements. If this occurs, then the sunlight simulator can be considered well calibrated. In the present study, the calculated values of photocurrent density were similar in both of the experiments (with a difference of less than 5%), confirming the quality of the calibrated sunlight simulator used.

From Table 1, it is possible to observe that TiNTs are widely used as catalysts for water splitting; however, in most cases, they are used as powders in photocatalytic reactions. Only a few studies applied TiNTs as photoanodes,[12,30,31] and in those cases, the obtained films were formed by randomly oriented TiNTs, and the potential for O_2 evolution was approximately 0.8 V, which is much higher than the value achieved in this work. Therefore, the synergic effect caused by the heterojunction of TiNTs and ZnONRs goes beyond lowering the charge recombination; it also enables the acquisition of a TiNT electrode without the agglomeration issue that can be used for the photoelectrocatalysis of water, generating O_2 at lower potentials than those reported previously in the literature.[12,30,31]

It could be thought that the utilization of multihierarchical electrodes based on TiO_2 nanomaterials, instead of titanate nanotubes, could result in better performance. Indeed the heterojunction of these two materials has been already reported, including: vertically aligned ZnONR films decorated with TiO_2 nanoparticles;[67] anodized TiO_2 nanotube/ZnONR hybrids;[14] or core–shell structures.[68] However, TiO_2 has a more negative conduction band than the ZnONRs, meaning that the photogenerated electrons would flow in the opposite way, from the ZnONRs to the TiO_2, resulting in less electrons flowing to the counter electrode and lower efficiency of the system. Therefore, the importance of using TiNTs to build these photoanodes is amplified, given rise to a new field of research, involving the improvement of the TiNT/ZnONR heterojunction.

Conclusions

Multihierarchical electrodes based on TiNT-decorated ZnONR films (TiNT → ZnONR) were reported for the first time. The materials were prepared by a simple two-step route. First, the hydrothermal synthesis of ZnONR films was performed; second, the films were stirred with the TiNT suspension. The amounts of TiNTs in the films are higher when glycine is added (to act as a bridge) either to TiNTs or to ZnONRs before mixing them to prepare the electrodes, obtaining TiNT + gly → ZnONR and TiNT → ZnONR + gly, respectively. The TiNTs were homogenously dispersed over the surface of the rods without forming agglomerates, which is common when other techniques for preparing TiNT films are used. Thus, we may be able to employ TiNTs to obtain photoanodes for water splitting experiments, which is highly unusual, once this material is applied in its powder form in photocatalysis experiments. The photoelectrocatalytic formation of H_2 and O_2 from water was evaluated by acquiring photocurrents *vs.* potential curves. Due to the synergic effect caused by the heterojunction of the TiNTs and ZnONRs, the recombination rate of the photogenerated charges was reduced, resulting in higher photocurrents compared with pure ZnONR films (0.9 mA cm^{-2} and 0.45 mA cm^{-2} at 1.23 V_{RHE}, respectively). Additionally, the potential for oxygen evolution is lower than the pure TiNT electrodes (0 V and 0.8 V *vs.* E_{RHE}, respectively), providing a good concept for further improvements of photocatalytic performance of metal oxide semiconductors. Further experiments are underway in our laboratory to optimize the synthesis protocol and to gain a better comprehension of the synergetic effects between TiNTs and ZnONRs to enhance their performance as photoanodes in PEC.

Acknowledgements

This work was supported by FAPESP (grant no. 2013/12997-0), INCT in Bioanalytics (FAPESP, grant no. 08/57805-2 and CNPq, grant no. 573672/2008-3), and CNPq (grant no. 472197/2012-6). J. S. S. acknowledges FAPESP (proc. no. 2011/17938-6 and 2013/07017-6) for fellowship grants. We are thankful to LNNano-CNPEM for the use of SEM facilities.

References

1 I. P. Jain, *Int. J. Hydrogen Energy*, 2009, **34**, 7368–7378.
2 K. Maeda and K. Domen, *J. Phys. Chem. Lett.*, 2010, **1**, 2655–2661.

3 A. Fujishima and K. Honda, *Nature*, 1972, **238**, 37–38.
4 T. Zhu, M. N. Chong and E. S. Chan, *ChemSusChem*, 2014, **7**, 2974–2997.
5 Y. Ling and Y. Li, *Part. Part. Syst. Charact.*, 2014, **31**, 1113–1121.
6 L.-w. Shan, G.-l. Wang, J. Suriyaprakash, D. Li, L.-z. Liu and L.-m. Dong, *J. Alloys Compd.*, 2015, **636**, 131–137.
7 V. M. Aroutiounian, V. M. Arakelyan and G. E. Shahnazaryan, *Sol. Energy*, 2005, **78**, 581–592.
8 D. V. Bavykin and F. C. Walsh, *Titanate and Titania Nanotubes: Synthesis, Properties and Applications*, Royal Society of Cheistry, London, 2010.
9 I. Gonzalez-Valls and M. Lira-Cantu, *Energy Environ. Sci.*, 2009, **2**, 19–34.
10 W. M. de Carvalho Jr and F. L. Souza, *J. Mater. Res.*, 2014, **29**, 16–28.
11 A. L. Stroyuk, I. V. Sobran and S. Y. Kuchmiy, *J. Photochem. Photobiol., A*, 2007, **192**, 98–104.
12 B.-R. Kim, H.-J. Oh, K.-S. Yun, S.-C. Jung, W. Kang and S.-J. Kim, *Prog. Org. Coat.*, 2013, **76**, 1869–1873.
13 F. L. Souza, K. P. Lopes, P. A. P. Nascente and E. R. Leite, *Sol. Energy Mater. Sol. Cells*, 2009, **93**, 362–368.
14 F.-X. Xiao, S.-F. Hung, H. B. Tao, J. Miao, H. B. Yang and B. Liu, *Nanoscale*, 2014, **6**, 14950–14961.
15 L. Zhu, M. Hong and G. W. Ho, *Sci. Rep.*, 2015, **5**, 11609.
16 M. Kitano, R. Mitsui, D. R. Eddy, Z. M. A. El-Bahy, M. Matsuoka, M. Ueshima and M. Anpo, *Catal. Lett.*, 2007, **119**, 217–221.
17 D. V. Bavykin, L. Passoni and F. C. Walsh, *Chem. Commun.*, 2013, **49**, 7007–7009.
18 S. Hyung-Shik, K. Gil-Sung, S. Hyung-Kee, V. P. Godble, K. Young-Soon and O. B. Yang, *Electrochem. Commun.*, 2006, **8**, 961–966.
19 W. Zhong Lin, *J. Phys.: Condens. Matter*, 2004, **16**, R829–R858.
20 G. C. Yi, C. R. Wang and W. I. Park, *Semicond. Sci. Technol.*, 2005, **20**, S22–S34.
21 X. Sheng and W. Zhong Lin, *Nano Res.*, 2011, **4**, 1013–1098.
22 D. Panda and T.-Y. Tseng, *J. Mater. Sci.*, 2013, **48**, 6849–6877.
23 J. L. Gomez and O. Tigli, *J. Mater. Sci.*, 2013, **48**, 612–624.
24 P. Lee, J. Ham, J. Lee, S. Hong, S. Han, Y. D. Suh, S. E. Lee, J. Yeo, S. S. Lee, D. Lee and S. H. Ko, *Adv. Funct. Mater.*, 2014, **24**, 5671–5678.
25 B. Yan, X. Li, Z. Bai, M. Li, L. Dong, D. Xiong and D. Li, *J. Alloys Compd.*, 2015, **634**, 50–57.
26 T. P. Gujarati, A. G. Ashish, M. Rai and M. M. Shaijumon, *J. Nanosci. Nanotechnol.*, 2015, **15**, 5833–5839.
27 H. M. Yeh, S. L. Lo, M. J. Chen and H. Y. Chen, *Water Sci. Technol.*, 2014, **69**, 1676–1681.
28 H. Dang, X. Dong, Y. Dong and J. Huang, *Int. J. Hydrogen Energy*, 2013, **38**, 9178–9185.
29 S. K. Parayil, J. Baltrusaitis, C.-M. Wu and R. T. Koodali, *Int. J. Hydrogen Energy*, 2013, **38**, 2656–2669.
30 C. Li, J. Yuan, B. Han, L. Jiang and W. Shangguan, *Int. J. Hydrogen Energy*, 2010, **35**, 7073–7079.
31 Y. J. Zhang, Y. C. Wang, W. Yan, T. Li, S. Li and Y. R. Hu, *Appl. Surf. Sci.*, 2009, **255**, 9508–9511.
32 Y. Zhang, Y. Wu, Z. Wang and Y. Hu, *Rare Met. Mater. Eng.*, 2009, **38**, 1514–1517.
33 K.-J. Noh, H.-J. Oh, H.-K. Ku, S.-C. Jung, W. Kang, S. Park and S.-J. Kim, *J. Nanosci. Nanotechnol.*, 2013, **13**, 1863–1866.
34 H.-J. Oh, K.-J. Noh, H.-K. Ku, K.-S. Park, S.-C. Jung, W.-J. Lee and S.-J. Kim, *J. Nanosci. Nanotechnol.*, 2011, **11**, 7210–7213.
35 Z. Kang, X. Yan, Y. Wang, Z. Bai, Y. Liu, Z. Zhang, P. Lin, X. Zhang, H. Yuan, X. Zhang and Y. Zhang, *Sci. Rep.*, 2015, **5**, 7882.
36 E. S. Babu, S.-K. Hong, V. Thanh Son, J.-R. Jeong and H. K. Cho, *Electron. Mater. Lett.*, 2015, **11**, 65–72.
37 Y. Wei, H. Du, J. Kong, X. Lu, L. Ke and X. W. Sun, *Electrochim. Acta*, 2014, **143**, 188–195.
38 M. Wu, W.-J. Chen, Y.-H. Shen, F.-Z. Huang, C.-H. Li and S.-K. Li, *ACS Appl. Mater. Interfaces*, 2014, **6**, 15052–15060.
39 K. Feng, W. Li, S. Xie and X. Lu, *Electrochim. Acta*, 2014, **137**, 108–113.
40 H. M. Chen, C. K. Chen, C.-J. Chen, L.-C. Cheng, P. C. Wu, B. H. Cheng, Y. Z. Ho, M. L. Tseng, Y.-Y. Hsu, T.-S. Chan, J.-F. Lee, R.-S. Liu and D. P. Tsai, *ACS Nano*, 2012, **6**, 7362–7372.
41 Y.-K. Hsu and C.-M. Lin, *Electrochim. Acta*, 2012, **74**, 73–77.
42 Y. Wei, L. Ke, J. Kong, H. Liu, Z. Jiao, X. Lu, H. Du and X. W. Sun, *Nanotechnology*, 2012, **23**, 235401.
43 Y. Hara, J. R. S. Brownson and M. A. Anderson, *Int. J. Appl. Ceram. Technol.*, 2012, **9**, 115–123.
44 D. V. Bavykin, E. V. Milsom, F. Marken, D. H. Kim, D. H. Marsh, D. J. Riley, F. C. Walsh, K. H. El-Abiary and A. A. Lapkin, *Electrochem. Commun.*, 2005, **7**, 1050–1058.
45 M. Klaumuenzer, A. Kahnt, A. Burger, M. Mackovic, C. Muenzel, R. Srikantharajah, E. Spiecker, A. Hirsch, W. Peukert and D. M. Guldi, *ACS Appl. Mater. Interfaces*, 2014, **6**, 6724–6730.
46 E. Smecca, A. Motta, M. E. Fragala, Y. Aleeva and G. G. Condorelli, *J. Phys. Chem. C*, 2013, **117**, 5364–5372.
47 M. Segovia, K. Lemus, M. Moreno, M. A. Santa Ana, G. Gonzalez, B. Ballesteros, C. Sotomayor and E. Benavente, *Mater. Res. Bull.*, 2011, **46**, 2191–2195.
48 H. Niu and Y. Cai, *Anal. Chem.*, 2009, **81**, 9913–9920.
49 N. Subramanian and A. Al Ghaferi, *RSC Adv.*, 2014, **4**, 4371–4378.
50 Y. K. Gao, F. Traeger, C. Woell and H. Idriss, *Surf. Sci.*, 2014, **624**, 112–117.
51 Q. Zhou, W. Chen, S. Peng and W. Zeng, *Sci. World J.*, 2014, 489170.
52 H. Liu, B. Huang, Z. Wang, X. Qin, X. Zhang, J. Wei, Y. Dai, P. Wang and M.-H. Whangbo, *J. Alloys Compd.*, 2010, **507**, 326–330.
53 Y. Chang, X. Liu, A. Cai, S. Xing and Z. Ma, *Ceram. Int.*, 2014, **40**, 14765–14768.
54 D. V. Bavykin, B. A. Cressey, M. E. Light and F. C. Walsh, *Nanotechnology*, 2008, **19**, 275604.
55 J. S. Souza, K. Krambrock, M. V. B. Pinheiro, R. A. Ando, S. Guha and W. A. Alves, *J. Mol. Catal. A: Chem.*, 2014, **394**, 48–56.
56 M. Guo, P. Diao and S. M. Cai, *J. Solid State Chem.*, 2005, **178**, 1864–1873.

57 D. V. Bavykin and F. C. Walsh, *J. Phys. Chem. C*, 2007, **111**, 14644–14651.
58 D. V. Bavykin, K. E. Redmond, B. P. Nias, A. N. Kulak and F. C. Walsh, *Aust. J. Chem.*, 2010, **63**, 270–275.
59 I. S. Grover, S. Singh and B. Pal, *Appl. Surf. Sci.*, 2013, **280**, 366–372.
60 X. Zou, H. Fan, Y. Tian and S. Yan, *Mater. Lett.*, 2013, **107**, 269–272.
61 Z. Zheng, Z. S. Lim, Y. Peng, L. You, L. Chen and J. Wang, *Sci. Rep.*, 2013, **3**, 2434.
62 M. Gateshki, Q. Chen, L.-M. Peng, P. Chupas and V. Petkov, *Z. Kristallogr.*, 2007, **222**, 612–616.
63 M. Ni, M. K. H. Leung, D. Y. C. Leung and K. Sumathy, *Renewable Sustainable Energy Rev.*, 2007, **11**, 401–425.
64 M. Gratzel, *Nature*, 2001, **414**, 338–344.
65 V. J. Babu, S. Vempati and S. Ramakrishna, *RSC Adv.*, 2014, **4**, 27979–27987.
66 Q. Li, H. Zhang, Z. Tu, J. Yu, C. Xiong and M. Pan, *J. Membr. Sci.*, 2012, **423**, 284–292.
67 V. Manthina, J. P. Correa Baena, G. Liu and A. G. Agrios, *J. Phys. Chem. C*, 2012, **116**, 23864–23870.
68 C. Xu, J. Wu, U. V. Desai and D. Gao, *Nano Lett.*, 2012, **12**, 2420–2424.